Structural Chemistry
https://doi.org/10.1007/s11224-022-02033-8

ORIGINAL RESEARCH

Targeting COVID-19 pandemic: in silico evaluation of 2-hydroxy-1, 2-diphenylethanone N(4)-methyl-N(4)-phenylthiosemicarbazone as a potential inhibitor of SARS-CoV-2

Rajan Jeevana[1] · Abu Pilakkaveettil Kavitha[2] · Thoppilan G. Abi[3] · Pookkottu K. Sajith[2] · Jibin K. Varughese[3] · Kuttamath Kunniyur Aravindakshan[4]

Received: 23 May 2022 / Accepted: 3 August 2022

Abstract

The global spread of the COVID-19 pandemic caused by the etiological agent, severe acute respiratory syndrome coronavirus-2 (SARS-CoV-2), triggered researchers to identify and develop novel antiviral therapeutics. Herein, we report a new molecule 2-hydroxy-1,2-diphenylethanone N(4)-methyl-N(4)-phenyl thiosemicarbazone (BMPTSC), as a potential inhibitor of SARS-CoV-2. BMPTSC was synthesized, characterized by IR and NMR studies, and the structural parameters were analyzed computationally by B3LYP/cc-pVDZ method. Molecular docking studies were performed to get insights into the energetics and compatibility of BMPTSC against various SARS-CoV-2 drug targets. The best docking poses of target protein-BMPTSC complex structures were further subjected to molecular dynamics (MD) simulations. Molecular mechanics Poisson–Boltzmann surface area (MM-PBSA) calculations on the binding of BMPTSC with the target proteins viz. spike glycoprotein and ACE-2 protein showed energy values of −179.87 and −145.61 kJ/mol, respectively. Moreover, BMPTSC obeys Lipinski's rule, and further in silico assessment of oral bioavailability, bioactivity scores, ADME, drug-likeness, and medicinal chemistry friendliness suggests that this molecule is a promising candidate for the COVID-19 drug discovery process.

Keywords SARS-CoV-2 · COVID-19 · Thiosemicarbazone · Molecular docking · Molecular dynamics · MM-PBSA · Pharmacokinetic properties

Introduction

Coronavirus disease 2019 (COVID-19), declared as a Public Health Emergency of International Concern (PHEIC) by the World Health Organization, is caused by a new strain of the virus which belongs to the order Nidovirales of the Coronaviridae family, named SARS-CoV-2 [1, 2]. The conventional therapeutic strategy to conquer viral infections is the inhibition of proteases which is essential for the proteolytic processing of viral polyproteins. SARS-CoV-2 genome encodes non-structural proteins (such as 3-chymotrypsin-like protease, papain-like protease, helicase, RNA-dependent RNA polymerase), structural proteins (such as spike glycoprotein), and accessory proteins. The non-structural proteins are the key enzymes in the viral life cycle, whereas the spike glycoprotein is essential for virus-cell receptor interactions during viral entry [1].

No part of SARS-CoV-2 is more vulnerable than its main protease, M^{pro}, which is essential to form a viral replication complex as it processes the huge polyproteins into which the viral RNA is initially translated once it enters the human cell [3]. The pivotal role played by this enzyme in mediating viral replication and transcription marks it as an excellent drug target for antiviral pharmacotherapy [4]. The availability of the crystallographic structure of

✉ Rajan Jeevana
jeevanarajan@gmail.com

✉ Abu Pilakkaveettil Kavitha
kavithayasir@gmail.com

✉ Thoppilan G. Abi
abitg@shcollege.ac.in

1 PG & Research Department of Chemistry, Govt. College, Madappally, Kozhikode 673102, Kerala, India

2 PG & Research Department of Chemistry, Farook College (Autonomous), Kozhikode 673632, Kerala, India

3 PG & Research Department of Chemistry, Sacred Heart College (Autonomous), Kochi 682013, Kerala, India

4 Department of Chemistry, University of Calicut, Malappuram 673635, Kerala, India

Published online: 17 October 2022

SARS-CoV-2 M^{pro} facilitates the rational design of lead compounds [5–7]. The literature survey depicts multiple projects focusing on the M^{pro} of the new coronavirus [4–13].

The auxiliary coronavirus protease, papain-like protease (PLpro), owing to the increased conservation of both position and sequences of polyprotein cleavage sites, could be exploited to develop selective inhibitors [1–3]. Studies have reported virtual screening of FDA-approved drugs against PLpro of novel coronavirus [14]. RNA viruses for genomic replication encode RNA-dependent RNA polymerase (RdRp). This enzyme, having conserved motifs with few exceptions, is also a challenging target [1]. Nsp15, endoribonuclease, is another potential drug target that aids in the virus's replication, possibly interfering with the host's immune response, and hence is essential in their life cycle and virulence. The inhibition of Nsp15 protein can slow down viral replication [15]. Accordingly, identifying Nsp15 inhibitors offers a better opportunity to design effective treatments for COVID-19.

The two functional subunits of spike glycoprotein, S_1 and S_2, are responsible for binding the virus to the host cell receptor [16]. The subunit S_1 contains the receptor binding domain, which enables the virus to bind to the host cell receptor, whereas the subunit S_2 is responsible for the binding to the host cell receptor through fusing the envelope of the virus with the host cell membrane. It was identified that angiotensin-converting enzyme 2 (ACE-2) is a crucial factor mediating the SARS-CoV-2 spike(S) protein's interaction with susceptible host cells, as the virus uses ACE-2 to enter host cells, replicate and spread. SARS-CoV-2 also enters target cells through an endosomal pathway using ACE-2 as the cell entry receptor. Therefore, these proteins function as attractive targets to identify potential drug candidates and develop antiviral agents against COVID-19.

Many in vitro [17, 18] and in silico studies, including both protein structure and ligand-based docking, have been reported to identify promising coronavirus inhibitors [19–21]. Using the molecular dynamics simulations, Abi and coworkers recently investigated the inhibitory activities of dietary flavonoids against SARS-CoV-2 [22]. They identified three dietary flavonoids, amentoflavone, naringin, and naringenin, as inhibitors of M^{pro} of novel corona virus after a virtual screening of thousands of bioactive compounds using molecular docking tools. Several studies have employed machine intelligence and deep learning strategies in designing COVID-19 drugs [23, 24].

Since no effective drugs are available for COVID-19 until the due date, a global emergency occurs to design and develop specific antiviral therapeutics. In this context, it would be worthwhile to identify SARS-CoV-2 inhibitors. It is well established that thiosemicarbazones, the first trustworthy antiviral agents synthesized, constitute an exciting class of compounds that stand as a milestone in the promising era of pharmacological applications [25, 26]. In addition, these compounds were found to be effective in humans and placed in clinical medicine [27, 28]. Besides the antiviral properties, these compounds have proved their biological activity as antioxidant [29, 30], antiparasitic [31–34], anticonvulsant [35], and antitumor [36–38] agents. During the past decades, thiosemicarbazones were clinically developed for various diseases, including tuberculosis, viral infections, malaria, and cancer [39]. 2-Acetylpyridine thiosemicarbazone derivatives inhibited the replication of herpes simplex virus types [40]. Vitamin-A-derived (retinoid) thiosemicarbazone was an excellent antiviral agent as proved by Kesel [41]. Antiviral activity of thiosemicarbazones derived from α-amino acids against Dengue virus was studied [42]. This class of compounds was also the focus of the first systematic studies on the relationship between chemical structure and antiviral activity [43]. The biological activity of such compounds depends on parent aldehyde or ketone [44, 45]. The presence of bulky groups at the N(4) position of the thiosemicarbazone moiety and an additional binding site significantly impacted biological activity [46]. Among the thiosemicarbazones, those with electron withdrawing substituents at N(4)-position have been studied extensively due to their promising biological activity [47, 48].

The present study includes the synthesis and structural analysis of a novel thiosemicarbazone, α-hydroxy ketone (benzoin) derivative of N(4)-methyl-N(4)- phenylthiosemicarbazide, abbreviated as BMPTSC, and computational evaluation for its SARS-CoV-2 inhibitory activity and important pharmacokinetic properties. The core computational study of protein–ligand (BMPTSC) binding interactions is performed using molecular dynamics (MD) simulations followed by molecular mechanics Poisson–Boltzmann surface area (MM-PBSA) calculations. We have performed druglikeness of BMPTSC and molecular docking of the ligand with various targets of SARS-CoV-2 before molecular dynamics simulations. The protein-BMPTSC-docked complexes with a docking score less than − 8.0 kcal/mol have been selected for molecular dynamics simulation studies. The results highlighted the potentiality of BMPTSC to inhibit ACE-2 and spike glycoprotein targets of SARS-CoV-2 effectively.

Materials and methods

Experimental details

In the present study, we synthesized α-hydroxy ketone (benzoin) derivative of N(4)-methyl-N(4)- phenylthiosemicarbazide, named BMPTSC.

Preparation of N(4)-methyl-N(4)phenylthiosemicarbazide (MPTSC)

MPTSC was prepared by modifying the procedure reported by Scovill et al. [49]. N-Methylaniline (10.7 cm^3, 0.1 mol) was dissolved in ammonia solution (20 cm^3), cooled in an ice bath, CS_2 (7.6 cm^3, 0.1 mol) was then added slowly to it, followed by ethanol (20 cm^3), and the solution was stirred in an ice bath for 2 h and allowed to stand for another 1 h. Sodium chloroacetate (10 cm^3 of 0.1 mol) was added, followed by a 50% hydrazine hydrate (10 cm^3), stirred well for 1 h, and kept aside overnight. Concentrated HCl (20 cm^3) was added. The compound precipitated out gradually and was filtered and washed with cold ethanol.

Synthesis of BMPTSC

Thiosemicarbazides readily condense with carbonyl compounds to form thiosemicarbazones in an alcohol medium. Benzoin (2.1 g, 0.01 mol) (Sigma Aldrich) and MPTSC (1.8 g, 0.01 mol) in 50 cm^3 ethanol were refluxed well for 2 h in the presence of 2 cm^3 of p-toluene sulfonic acid as a catalyst on a water bath. The mixture was concentrated to reduce the volume to half and kept for half an hour. The yellow precipitate formed was filtered and washed with cold ethanol (m.p. 116 °C).

The follow-up of the reaction rates was performed by thin-layer chromatography (TLC) on glass sheets precoated with silica gel, and the spots were visualized by exposure to iodine vapors. The percentages of carbon, hydrogen, and nitrogen in the compound were determined using a Hitachi CHN rapid analyzer and that of sulfur by Kjeldahl's method. The IR spectra of the compound using KBr disks were recorded on a Shimadzu FTIR-8101A spectrophotometer with a scanning range of 400–4000 cm^{-1}. ^1H NMR spectrum of the compound was recorded in DMSO-d_6 by using 300 MHz Bruker Advanced DPX spectrometer. The data were recorded as chemical shifts expressed in δ (ppm) relative to tetramethylsilane (TMS) as the internal standard. ^{13}C NMR spectrum of the compound was recorded in DMSO using a Bruker NMR spectrometer.

Computational details

The geometry optimization of BMPTSC was performed at the B3LYP/cc-pVDZ [50, 51] level of theory with Gaussian 09 software package [52]. The compound was further subjected to in silico studies, including molecular docking, molecular dynamics simulations, screening of oral bioavailability, and bioactivity scores against various drug targets using Molinspiration online software [53], and ADME (absorption, distribution, metabolism, excretion) and medicinal chemistry friendliness properties using Swiss ADME webserver [54].

Molecular docking

The molecular docking calculations were carried out using Autodock Tools and Vina scoring functions [55]. Six targets of SARS-CoV-2 were used for molecular docking studies, namely, spike glycoprotein (PDB ID: 6VXX), main protease, Mpro (PDB ID: 6YB7), endoribonuclease, Nsp15 (PDB ID: 6VWW), RNA-dependent RNA polymerase, RdRp (PDB ID: 6M71), papain-like protease, PLpro (PDB ID: 6W9C), and angiotensin-converting enzyme-2, ACE-2 (PDB ID: 1R42). We also performed the docking studies of the target proteins mentioned above with five standard drugs: antimalarial drugs such as chloroquine and hydroxychloroquine, and antiviral drugs like ribavirin, cidofovir and favipiravir.

The crystal data of all the target protein structures were retrieved from Protein Data Bank (https://www.rcsb.org/). The initial preparation of these PDB structures was carried out by removing water and co-crystallized ligands, followed by the addition of missing hydrogens and charges. The Cartesian coordinates of the binding sites of the selected targets, viz., 1R42, 6VXX, 6YB7, 6VWW, 6M71, and 6W9C, are located as follows: (i) $x = 54.703$, $y = 59.927$, $z = 29.08$ (ii); $x = 210.298$, $y = 211.528$, $z = 214.946$ (iii); $x = 8.219$, $y = 0.586$, $z = -4.765$ (iv); $x = -62.418$, $y = 23.009$, $z = -19.046$ (v); $x = 139.275$, $y = 134.835$, z = 156.784, and (vi) $x = -35.427$, $y = 30.38$, $z = 7.021$, respectively. The minimum energy geometry of BMPTSC obtained from the B3LYP/cc-pVDZ level of theory was adopted for the docking calculations. The grid box used was of $40 \times 40 \times 40$ size. The grid point spacing and exhaustiveness used in these calculations are 1 and 8 Å, respectively. The results were compared with those of five standard medications including two antimalarial drugs such as chloroquine and hydroxychloroquine and three antiviral drugs such as cidofovir, favipiravir, and ribavirin; the structures of those were downloaded from PubChem [56]. Binding affinity scores (kcal/mol) of BMPTSC and other drugs with the binding sites of various SARS-CoV-2 targets were calculated. In addition, the results were validated by docking simulations using AutoDock 4.2 [57]. Furthermore, we analyzed the docking results using Discovery Studio Visualizer [58].

Molecular dynamics simulations and MM-PBSA calculations

All MD simulations were performed with the Gromacs 5.1.5 software package [59]. The OPLS force field and SPC/E, respectively, were used to simulate the protein–ligand system and water molecules [60–62]. The structures (best docking poses) of BMPTSC complexed with the target proteins spike

glycoprotein, ACE-2 protein, endoribonuclease, and Mpro are only preceded to MD simulation studies on account of its docking ranks with binding energy less than −8.0 kcal/mol. The evolution of the solvated protein–ligand system with respect to time was calculated using the default Verlet integrator [63] within the Gromacs code. Two fs time step was fixed to execute the equilibration and production MD run. The long-range electrostatic forces in the simulating system were constrained using the particle-mesh Ewald (PME) summation method [64]. The parameter associated with rigid bonds in the protein–ligand residues was maintained using linear constraint solver (LINCS) algorithm [65]. The temperature and pressure of the system were maintained at 300 K and 1 bar, respectively. The MD simulation of the protein–ligand complex in water involves energy minimization and 1-ns NVT-NPT equilibration followed by a 150-ns production run with periodic boundary conditions. The coordinates of MD trajectory were written at every 10 ps to get enough conformations for sampling and analysis. The MD trajectory sampling was used to assess the protein–ligand nonbonding interactions. Proper equilibration of the simulating system was monitored using the tools of potential energy analysis, temperature/pressure calculations, RMSD, and RMSF.

The MM-PBSA method was extensively used to estimate binding free energies of ligand in the target proteins by using molecular mechanics calculations and continuum solvation models [66, 67]. We performed the MM-PBSA calculations of selected snapshots obtained from sampling single MD trajectory within the formalism of g_mmpbsa methodology [68]. The binding free energy of a ligand inside a protein–ligand complex is calculated using the following expression:

$$\Delta G_{bind} = G_C - \left(G_P + G_L\right) \tag{1}$$

The individual free energy components of the expression (1) are further explained as follows:

$$G = E_{MM} + G_{solv} - TS$$

$$E_{MM} = E_{bonded} + E_{elec} + E_{vdW} \tag{2}$$

The molecular mechanics potential (E_{MM}) is calculated as the sum of bonding and nonbonding (van der Waals + electrostatic) terms. The entropy term (TS) in the above expression is neglected in the current methodology as we are focusing on the relative binding energy.

$$G_{solv} = G_{PB} + G_{SA} \tag{3}$$

The free energy of solvation (G_{solv}) is a combination of Poisson-Boltzmann equation (G_{PB}) term of polar interactions and (G_{SA}), a nonpolar free energy term of solvent-accessible surface area (SASA). The solvent dielectric constant and solvent probe radius in the g_mmpbsa calculation was fixed as 80 and 1.4 Å, respectively. We have carried out g_mmpbsa calculations by utilizing snapshots of equilibrated 120–150-ns trajectory at 100-ps intervals. The reported binding energy and its energy subcomponents were from the MM-PBSA calculations, followed by binding energy per residue decomposition analysis [69, 70].

Screening of oral bioavailability, bioactivity scores, ADME, druglikeness, and medicinal chemistry friendliness properties

The physicochemical properties of BMPTSC, required to determine the oral bioavailability, an important pharmacokinetic property, were computed using Molinspiration online software (http://www.molinspiration.com/). This is validated by applying the Lipinski's rule of five [71], according to which good oral bioavailability is ensured if a drug candidate satisfies: (a) a molecular mass less than 500 Daltons, (b) an octanol–water partition coefficient, logP, not greater than 5, (c) the number of hydrogen bond donors (-OH and -NH groups), less than 5, and (d) no more than 10 hydrogen bond acceptors (N and O atoms). It describes a compound to be orally active as long as not more than one rule is violated. There are exceptions to Lipinsk's rule of five, such as polar surface area should be less than or equal to 140 $Å^2$, and the number of rotatable bonds should be less than or equal to 10.

Molecular polar surface area, calculated as a sum of fragment contributions, is a good indicator of drug absorption, which includes intestinal absorption, blood–brain barrier penetration, bioavailability, and Caco-2 permeability, which is related to the hydrogen bonding potential of a molecule describing the drug permeability [72–74]. The number of rotatable bonds, given by the number of single non-ring bonds bounded to non-terminal heavy (non-hydrogen) atoms, is a measure of molecular flexibility [75]. Molecular volume is an essential parameter in determining the transport characteristics of a molecule, such as intestinal absorption and blood–brain barrier penetration.

The bioactivity of BMPTSC was investigated for important drug classes, such as GPCR ligand, ion channel modulator, kinase inhibitor, nuclear receptor ligand, protease inhibitor, and enzyme inhibitor, with the help of Molinspiration Bioactivity Score V 2018.03. A positive bioactivity score indicates considerable bioactivity, whereas a score ranging from − 0.5 to 0.0 indicates moderate activity, and less than −0.5 depicts inactive nature.

ADME properties, including lipophilicity, water solubility, pharmacokinetics, druglikeness, and medicinal chemistry friendliness, were computed using SwissADME, a free web tool providing free access to a pool of fast and robust predictive models for various properties to be satisfied by a drug-like molecule [54]. The server offers five predictive

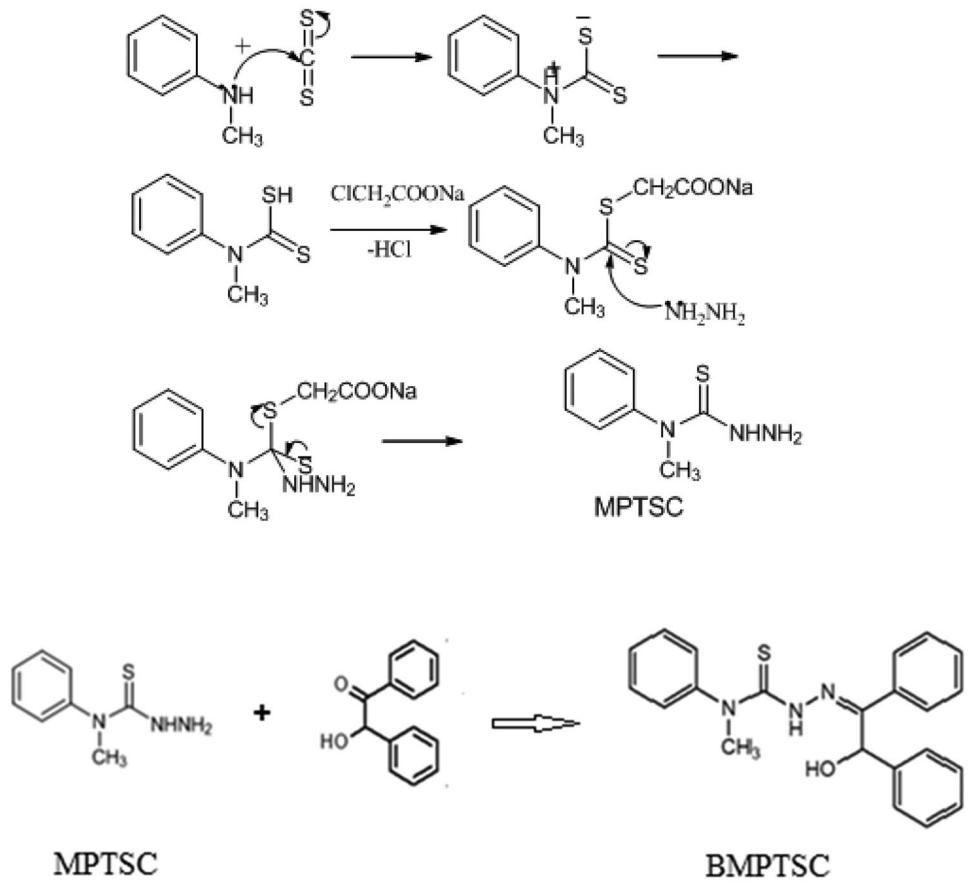

Fig. 1 The synthetic routes adopted to obtain the desired target compound

models, viz. (iLOGP), XLOGP, WLOGP, MLOGP, and SILICOS-IT, to calculate a molecule's lipophilicity in terms of partition coefficient between n-octanol and water. The web tool offers three topological methods to evaluate solubility: Esol model, Ali mode, and SILICOS-IT. It also permits the computation of various parameters essential for explaining gastrointestinal absorption, blood brain barrier (BBB) permeation, inhibitive nature against various enzymes, bioavailability score, druglikeness, lead likeness, and synthetic accessibility.

Results and discussion

Experimental details

The scheme of synthetic routes adopted to obtain the desired target compound is outlined in Fig. 1; the corresponding physical and analytical data are presented in Table 1.

BMPTSC is a yellowish powder with m.p. 116 °C, and yield is about 80%. The elemental analysis of the compound shows good agreement between the observed and calculated values of the percentage of carbon, hydrogen, nitrogen, and sulfur in BMPTSC, as given in Table 1. The IR spectrum of the compound revealed absorption bands at ν (cm^{-1}): 3415 assigned for O–H, 3379 for N–H, 1590 for C = N, 1205 for C-O, and 810 for C = S groups. Prominent ^{1}H NMR assignments of the molecules are as follows: ^{1}H-NMR (300 MHz, DMSO-d_6): δ 5.9 (–NH), δ 4.1 (–CH), δ 2.2 (combination of -OH and -NCH_3 protons), and δ 1.3 (–SH). The multiplet observed between 7.2 and 8.0 ppm in the spectrum of BMPTSC has been assigned to C_6H_5 protons. The spectrum of the compound showed a broad signal at 2.2 ppm. It is attributed to the combination of –OH and -NCH_3 protons merged into one signal. The signal at 4.1 ppm in the spectrum is due to the –CH proton of –CHOH of benzoin. A sharp singlet at 5.9 ppm in the spectrum of the ligand is assignable to –NH proton. The signal at 1.3 ppm is due to –SH proton. The ^{13}C-NMR chemical shifts for carbon atoms of C = S, C = N, CH-OH, and N-CH_3 groups are 196.9, 167.3,117.2, and 45.17 ppm, respectively. The carbon in the phenyl ring shows a chemical shift between 127 and 135 ppm. IR, ^{1}H-NMR, and ^{13}C-NMR spectra of BMPTSC are given in the supporting information (Figs. S1, S2, and S3).

Table 1 Physical and analytical data of BMPTSC

Compound	Color	Yield (%)	Melting point/decomposition temp. (°C)		Elemental analysis (%)			
					C	H	N	S
BMPTSC	Yellow	80	116	Observed	69.88	5.12	10.88	8.11
				Calculated	70.42	5.61	11.21	8.56

Optimized geometry of BMPTSC

Presented in Fig. 2 is the optimized geometry of the BMPTSC molecule calculated at the B3LYP/cc-pVDZ level of theory. The important structural parameters of the compound are listed in the supporting information. The optimized geometry of BMPTSC is used for further computational analysis, such as the initial geometry of molecular docking analysis, calculation of oral bioavailability and bioactivity scores against various drug targets, ADME (absorption, distribution, metabolism, excretion), and medicinal chemistry friendliness properties.

Molecular docking studies

The molecular docking results were analyzed based on binding affinity and protein–ligand interactions at the binding site. It can be seen that BMPTSC showed the highest affinity

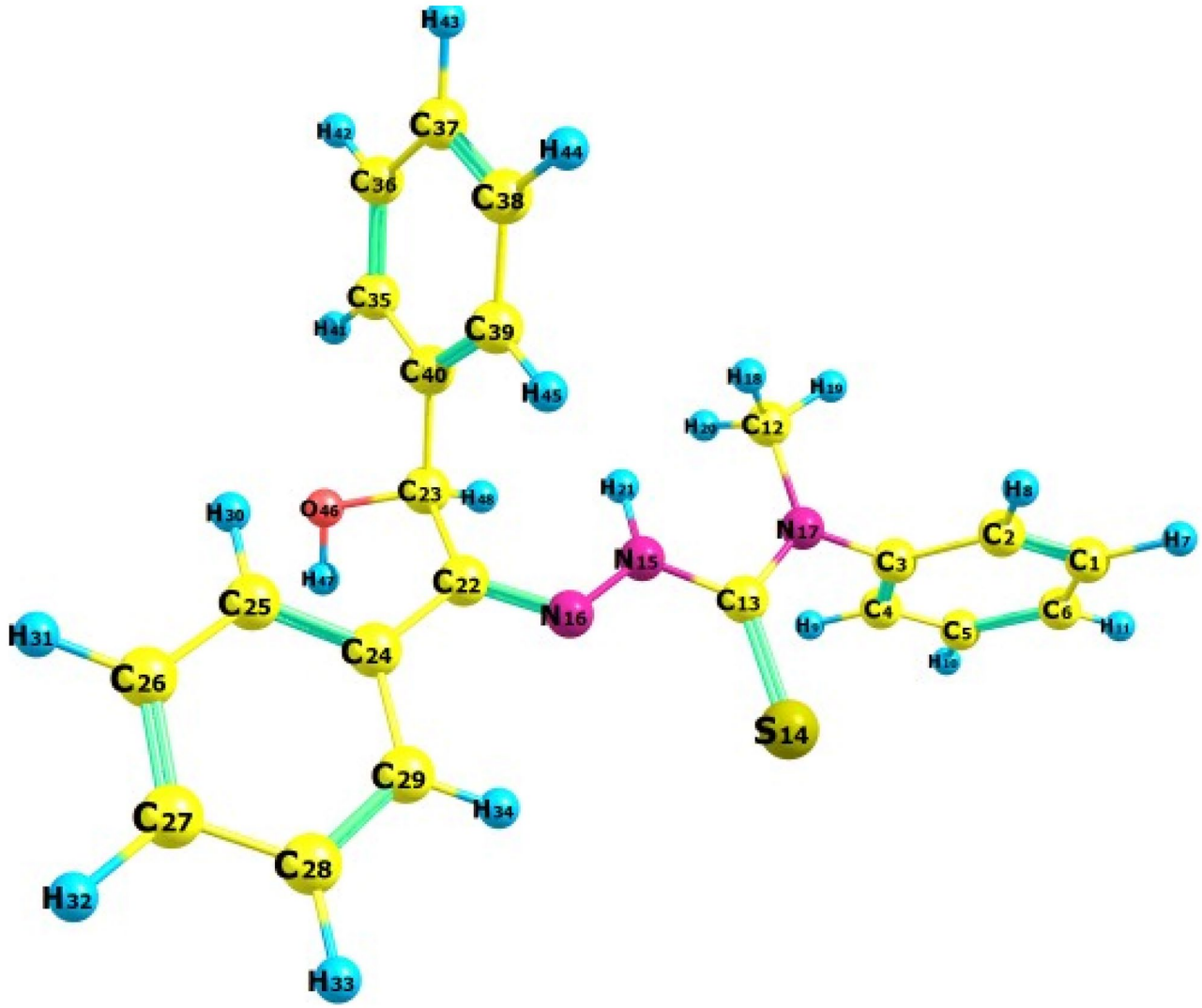

Fig. 2 Optimized geometry of BMPTSC

with targets such as ACE-2 and spike glycoprotein with a binding score of −8.4 and −8.3 kcal/mol, respectively. It also exhibits a strong binding affinity with Mpro and Nsp15 with a score of −8.1 kcal/mol. The title compound is found to have undergone considerable binding with RdRp and PLpro targets, as revealed by the binding affinities −7.2 and −7.0 kcal/mol, respectively. The docking results exemplify the crucial role of BMPTSC for its potential inhibitory activity against ACE-2, spike glycoprotein, main protease, and endoribonuclease targets of SARS-CoV-2. Table 2 presents the binding affinity scores of BMPTSC and other drugs with different SARS-CoV-2 targets.

BMPTSC is exhibiting a better binding affinity score with all the targets than standard drugs, which clearly depicts the enhanced potential of BMPTSC to inhibit these coronavirus targets, as compared with chloroquine, hydroxychloroquine, ribavirin, cidofovir, and favipiravir. The study highlights the versatility of BMPTSC as a promising candidate for coronavirus drug discovery. The docking simulations further validated the results.

The best pose of docked state and 2D diagrams depicting the characteristic binding interactions of BMPTSC at the active site of various targets is shown in Figs. 3 and 4, respectively. 2D diagrams illustrating the typical binding interactions of ribavirin, chloroquine, hydroxychloroquine, cidofovir, and favipiravir, at the active site of the selected targets are given in the supporting information (Figs. S4, S5, S6, S7, and S8).

Target protein-BMPTSC interactions have been analyzed in each case since binding affinity and drug efficacy rely on such interactions, which involve weak intermolecular interactions such as hydrogen bonding and hydrophobic interactions as the key players in stabilizing a small molecule energetically in the binding pocket of a protein structure [76–78]. Analysis of docking interactions reveals that BMPTSC has formed hydrogen bonds with all the selected targets. Only one hydrogen bond is formed between BMPTSC and 6VXX (Gln 1010), while it formed two hydrogen bonds each with ACE-2 (Ser 44, Asp 350), 6YB7 (Asp 197, Lys 137), 6VWW (Lys 90, Asp 273), 6M71 (Met 129, Tyr 149), and 6W9C (Thr 9, Gln 19).

Besides hydrogen bonding, favorable interactions such as hydrophobic, π-π stacking, and salt bridge have also been involved between BMPTSC and the targets of interest. BMPTSC shows π-π interactions with Phe 40, Trp 349, and Phe 390 residues of the 1R42 target, along with one favorable interaction with Asp 350 residue. The studied compound interacted with 6VXX using two carbon-hydrogen bonds with Gln 954 and Glu 1017 residues and one π-σ interaction with Gln 954 residue. For BMPTSC-6YB7 binding, two C-H bonds are formed with the residues, Asp 197 and Thr 198, one π-σ interaction with Leu 286, and two pi-alkyl interactions with Lue 286 and Lys 137 residues, along with π-anion and salt bridge with the residue Glu 290. Also, there exists one favorable attractive interaction with Asp 289.

6VWW- BMPTSC interactions involve the following: C-H bond (Arg 199), π-π stacked (Tyr 279), π-alkyl (Leu 201 and 252, Lys 90 and 277), π-anion, and favorable attractive interaction (Asp 268). The binding of BMPTSC in the bioactive core of 6M71 has been explained by the existence of π-σ (Leu 122 and 128), π-π stacked (Tyr 149), and π-alkyl (Ala 125, Leu 128, and Val 130), along with two hydrogen bonds, as mentioned earlier. The interactions involving π-anion (Asp 61), π-alkyl (Leu 64 and Val 57) and π-π stacked (His 17), account for the binding of BMPTSC in the binding pocket of the target, 6W9C.

To sum up, the compound under study has bound into the active sites of various targets used, with various protein–ligand interactions; out of which, hydrogen bonding and hydrophobic interactions predominate.

Out of the six targets employed for the docking study, four exhibited binding affinity scores above −8.0 kcal/mol, which are 1R42, 6VXX, 6YB7, and 6VWW, with binding affinity scores of −8.4, −8.3, −8.1, and −8.1 kcal/mol, respectively. These four best protein-BMPTSC pairs were used for MD simulation.

MD trajectory analysis and non-bonding interactions

The results obtained from the post-MD analysis of four protein–ligand systems are discussed in this section. The RMSD plot of complex (protein + ligand) and protein structure during the course of the simulation with respect to their initial structures are presented in Fig. 5a,

Table 2 Binding affinity scores of BMPTSC and other drugs with different SARS-CoV-2 targets. All values are in kcal/mol

Compound	1R42	6VXX	6YB7	6VWW	6M71	6W9C
BMPTSC	−8.4	−8.3	−8.1	−8.1	−7.2	−7.0
Ribavirin	−7.2	−8.2	−7.8	−7.9	−5.7	−7.2
Chloroquine	−7.6	−7.6	−7.4	−7.6	−5.7	−6.1
Hydroxychloroquine	−7.8	−7.6	−7.4	−7.5	−5.9	−6.4
Cidofovir	−6.8	−7.8	−7.3	−7.1	−5.0	−6.0
Favipiravir	−5.8	−6.3	−7.6	−6.6	−4.9	−6.5

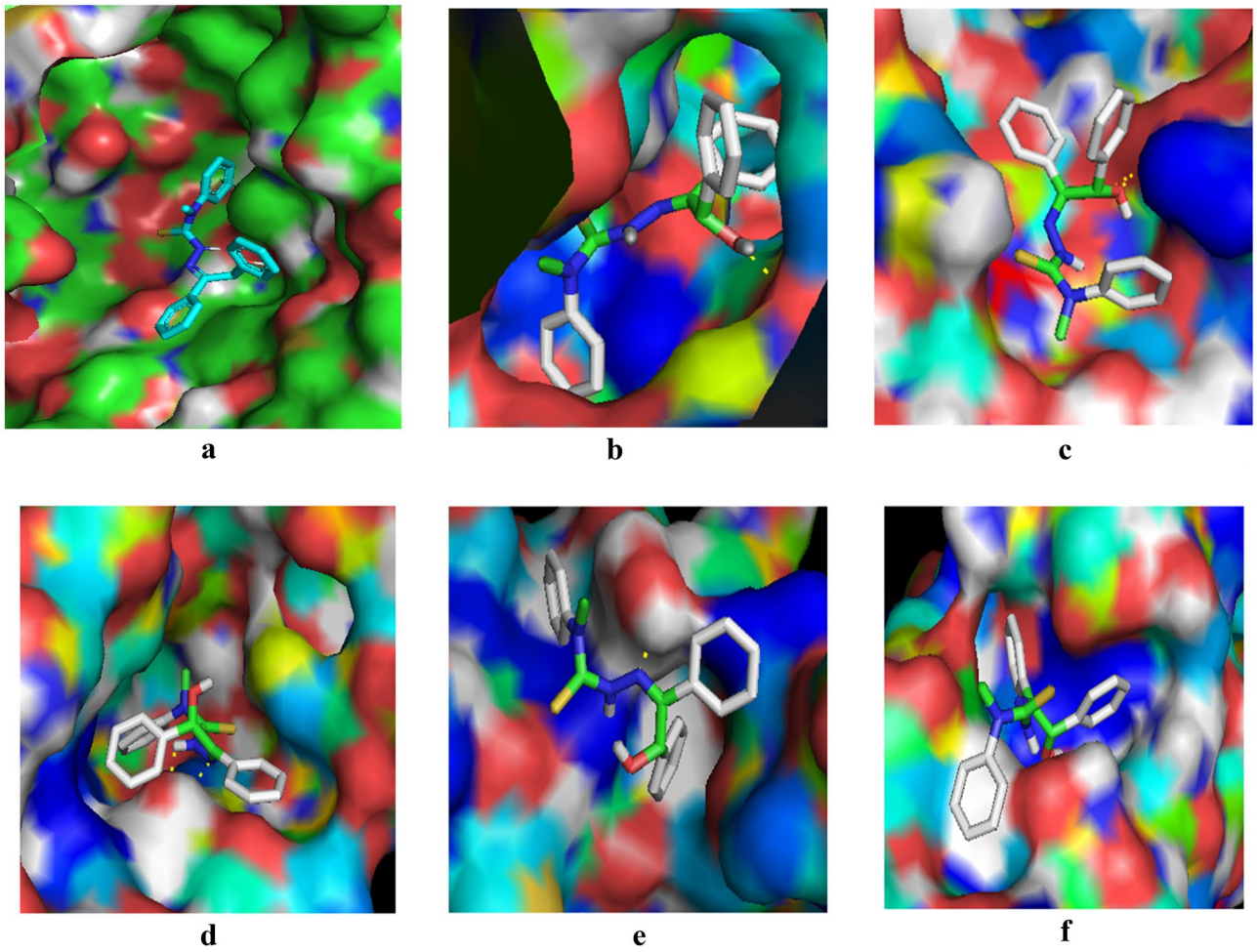

Fig. 3 Docked poses of BMPTSC with various targets with PDB ID: **a** 1R42, **b** 6VXX, **c** 6YB7, **d** 6VWW, **e** 6M71, **f** 6W9C

b respectively. It can be seen that the RMSD of all protein structures (Fig. 5b) lies within 0.3 nm with slight fluctuations for spike-glycoprotein (6VXX) and ACE-2 (1R42). In the same 150-ns MD trajectory, the RMSD of all complex structures (Fig. 5a) was found to be stabilized within the range of 0.4 nm with minimum fluctuations (particularly at 100–150-ns interval). This is an indication of stable protein–ligand complex formation in all solvated systems.

Next, we evaluated the contribution of all protein–ligand residues to the conformational changes of all complexes in the MD trajectory as root mean square fluctuations (RMSF) and is presented in Fig. 6. Almost all the amino acid residues of both chains (A and B) of spike glycoprotein show an average fluctuation of 0.54–0.56 nm (Fig. 6a). Except some terminal residues, the residues of all other targets (Fig. 6b–d) are highly conserved during the production run with a minimum fluctuation of ≤ 0.2. The ligand (BMPTSC) residue exhibits comparatively more fluctuations than protein residues in all protein–ligand complexes except (0.23) nm in the case of Nsp15 complex (LIG348, Fig. 6b). The RMSF value of ligand (BMPTSC) residue in spike glycoprotein (LIG1024, Fig. 6a), ACE-2 (LIG348, Fig. 6c), and Mpro (LIG307, Fig. 6d) complexes was found to be 0.77, 0.74, and 0.75 nm respectively. When we calculated the RMSF of protein alone, a similar quantity of fluctuations was observed in the protein residues of all systems. Less percentage of fluctuating protein-residues in the MD simulations was again an indication of stable protein–ligand systems. Furthermore, the stability and compactness of protein structure in the simulating protein–ligand system are verified using a radius of gyration (provided in the Supporting Information).

We further analyzed the MD trajectories with the PyContact tool to understand the presence of hydrogen bonding and hydrophobic interactions in the protein-BMPTSC complexes [79, 80]. The cutoff distances for hydrogen bonding and hydrophobic contact are fixed to be 3.0 and 4.5 Å, respectively. Figure 7 displays the details of hydrophobic and hydrogen-bonding interactions present in the protein-BMPTSC complexes. As indicated in Fig. 7a, b, the BMPTSC ligand shows consistent hydrogen bonding

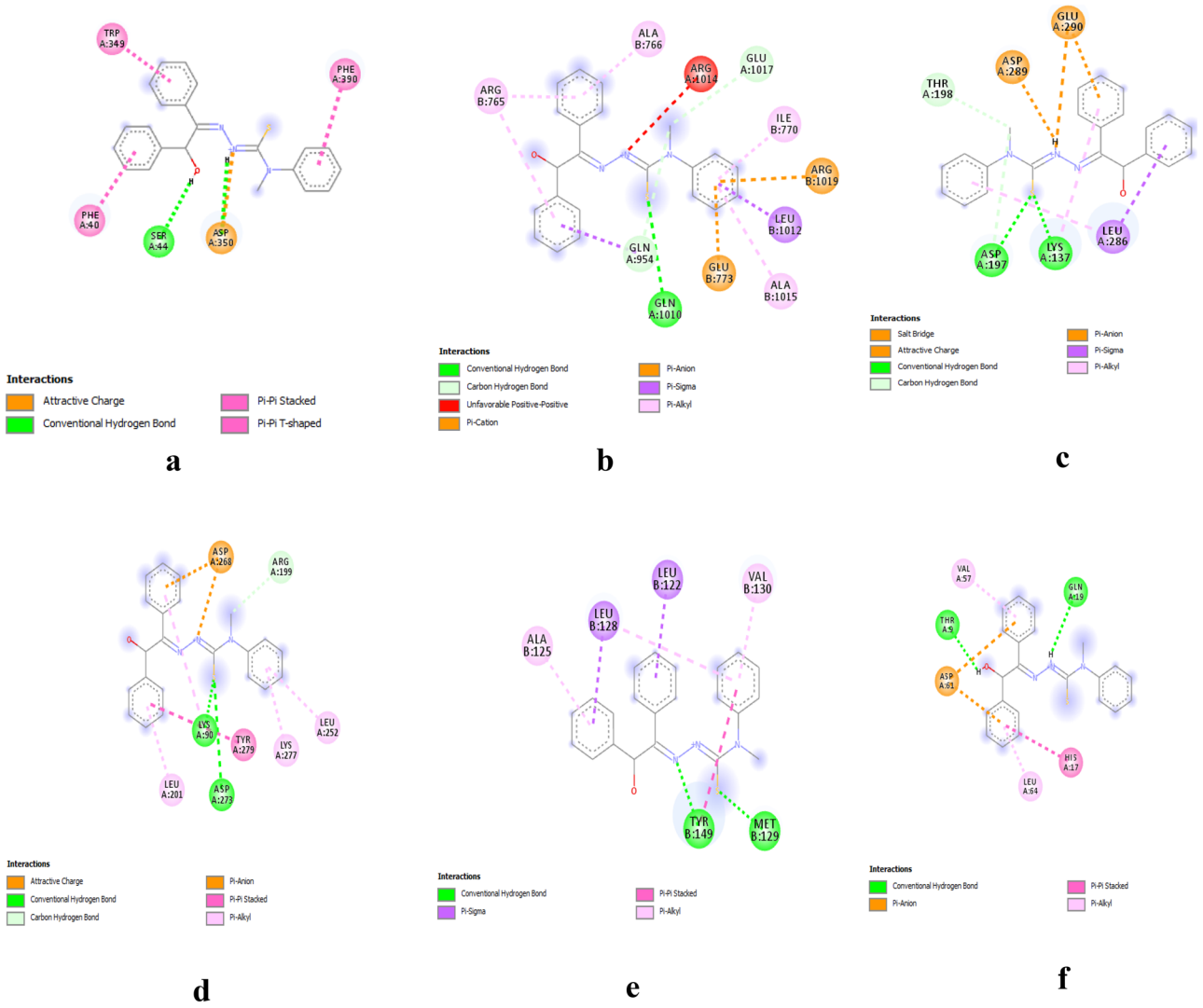

Fig. 4 2D diagrams showing interactions of BMPTSC with various targets with PDB ID: **a** 1R42, **b** 6VXX, **c** 6YB7, **d** 6VWW, **e** 6M71, **f** 6W9C

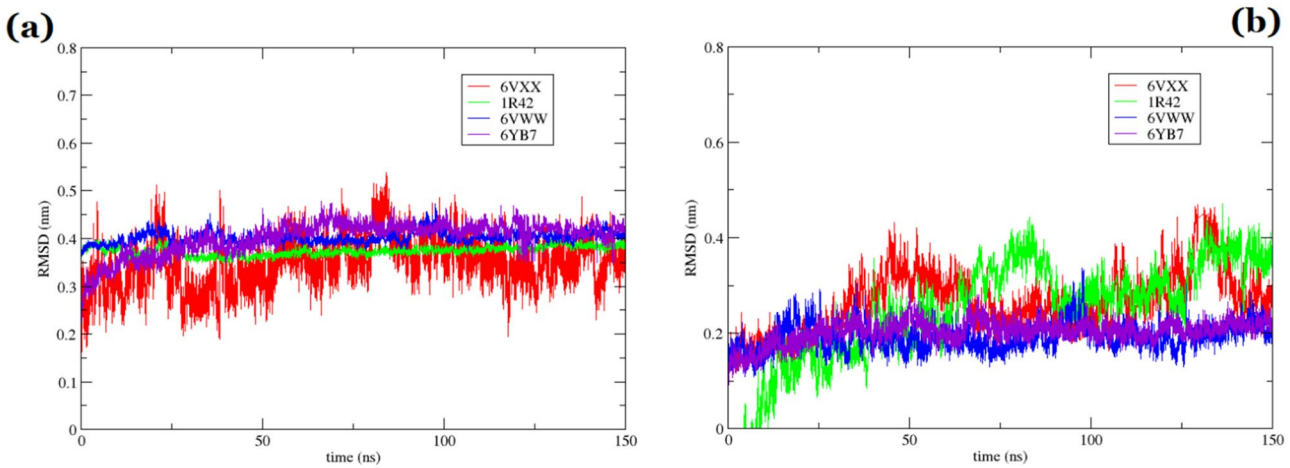

Fig. 5 RMSD plots of **a** all protein complex structures and **b** all protein structures

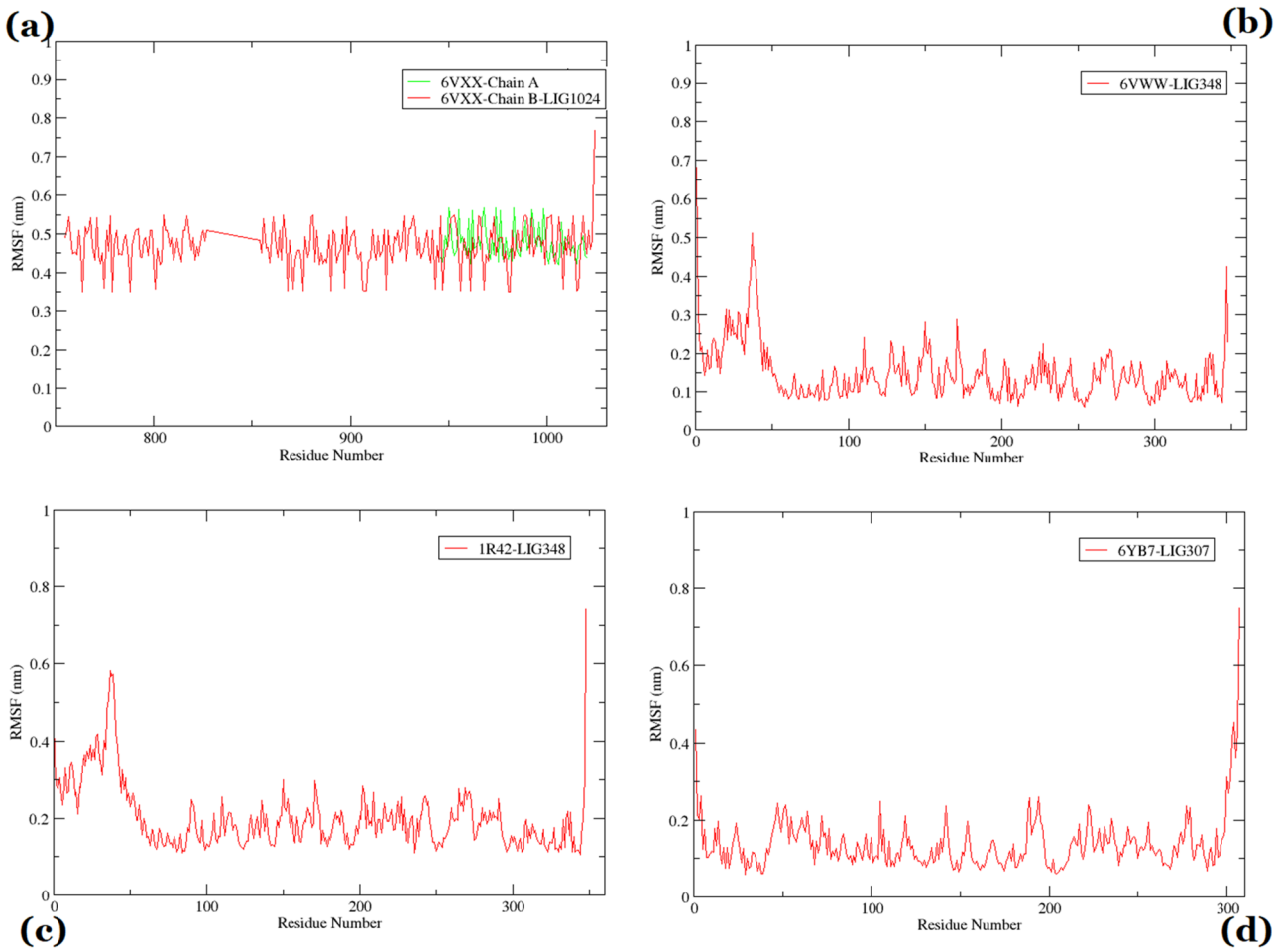

Fig. 6 RMSF plot of protein–ligand residues in **a** spike glycoprotein (6VXX), **b** Nsp15 (6VWW), **c** ACE-2 (1R42), and **d** MPro (6YB7) complexes

interactions as well as hydrophobic interactions with active site amino acid residues of spike glycoprotein. The amino acid residues TYR1007, LEU962, ARG1017, and GLN954 of chain A of spike glycoprotein have strong hydrophobic contacts with BMPTSC with more than 50% occupancy during the 150-ns MD trajectory. Meanwhile, GLN1010 residue of chain A and ARG765 of chain B of spike protein has strong hydrogen bonding interactions with occupancy

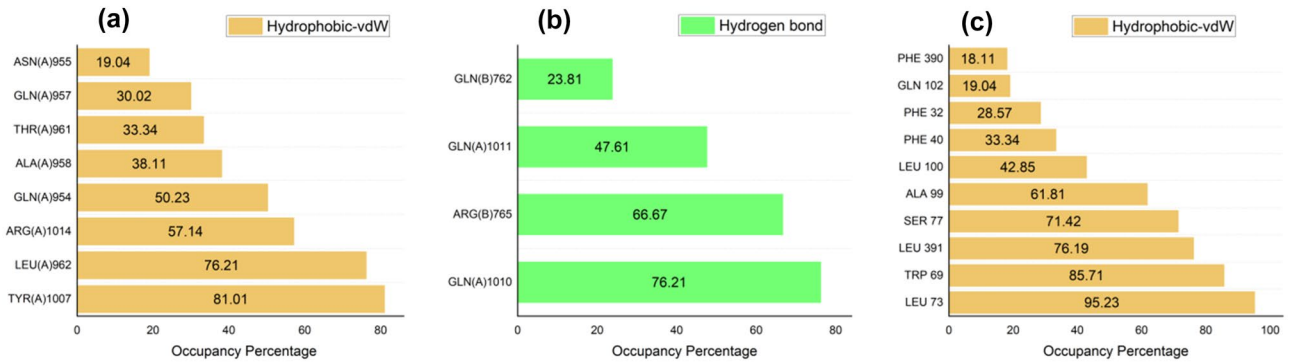

Fig. 7 Protein-BMPTSC nonbonding interaction profile. **a** and **b** corresponding to the hydrophobic and hydrogen bond interactions present in the spike complex of glycoprotein–BMPTSC, respectively, whereas **c** for hydrophobic interaction in ACE-2–BMPTSC pairs

above 50%. On the other hand, BMPTSC has only significant hydrophobic interactions with residues of ACE-2 protein, as illustrated in Fig. 7c. The active site amino acid residues LEU73, TRP69, LEU391, SER77, and ALA99 of ACE-2 target exhibit strong hydrophobic contacts with BMPTSC ligand on account of its occupancy above 50%. We also noted that no such consistent hydrogen bond and hydrophobic interactions are present in the Nsp 15 and Mpro protein-BMPTSC complexes. The knowledge of active site residues with nonbonding interactions is helpful for the analysis of binding free energy obtained from MM-PBSA calculations.

MM-PBSA binding energies

The binding free energies of four protein complexes are calculated by MM-PBSA analysis. The MM-PBSA analysis has emerged as an effective tool to partition the total free energy of protein–ligand binding into its various fragments, namely, electrostatic, polar solvation energy, and nonpolar solvation energy. This type of analysis is generally called energy decomposition analysis and the results are tabulated in Table 3, along with the binding free energy values. We also performed the ligand residue free energy decomposition analysis of the protein–ligand complex using the MM-PBSA method. MM-PBSA results are obtained by utilizing the 300 snapshots from the equilibrated MD trajectory (120–150-ns interval). We confirmed the MM-PBSA results presented in Table 3 by repeating the calculations on 5 sets of MD replicates of 10 ns duration, and the results are provided in the supporting information. The potential binding of BMPTSC ligand to the active site of spike glycoprotein, ACE-2 protein, Nsp15, and Mpro in terms of MM-PBSA binding free energies are −179.84, −145.6, −93.9, and −55.6 kJ/mol, respectively. The binding free energy values obtained indicate that BMPTSC is a potential inhibitor of spike glycoprotein, followed by ACE-2 protein.

The pictorial representation of protein residue contribution towards the MM-PBSA binding energy is presented in Fig. 8. The term hot spot residue (or red spot residue) generally indicates those amino acid residues stabilizing the protein–ligand complex with significant negative energy values (< −5.0 kJ/mol) towards the MM-PBSA binding free energy. In contrast, bad-contact residues, also called blue spot residues, contribute positive energy values to the MM-PBSA binding energy. Figure 9 displays the red spot and blue spot residues in protein-BMPTSC complexes. The ligand residue contribution to the MM-PBSA binding energy for spike glycoprotein, ACE-2 protein, NSP protein, and Mpro targets is −100.03, −62.03, −53.9, and −33.4 kJ/mol, respectively.

Based on the potential binding of BMPTSC on spike glycoprotein and ACE-2 protein, we extended our analysis to the hot spot residues of those proteins that contribute to the MM-PBSA binding energies through nonbonding interactions such as hydrophobic and hydrogen bonding interactions. van der Waal interactions (or hydrophobic interactions) are generally superior to hydrogen-bonded interactions in protein–ligand complexes. A similar trend is reflected in our calculations as van der Waal energy contributed with a significant negative value to the total binding energy.

For the spike protein-BMPTSC complex, TYR(A)1007 is the crucial amino acid residue that significantly contributes (−10.57 kJ/mol) to the binding free energy through hydrophobic interaction. The other red spot residues with energy contributions are ALA(A)958 (−10.3 kJ/mol), GLN(A)1010 (−9.4 kJ/mol), GLN(A)1011 (−6.2 kJ/mol), GLN(A)957 (−5.0 kJ/mol), ASN(A)955 (−4.4 kJ/mol), LEU(A) 962 (−4.1 kJ/mol), and GLN(A)762 (−2.5 kJ/mol) respectively. As indicated in the protein-BMPTSC nonbonding interaction profile (Fig. 6), the residues ALA(A)958, GLN(A)957, ASN(A)955, and LEU(A) 962 interact with BMPTSC through hydrophobic interactions. Hydrogen bonding or electrostatic interactions contribute next to van der Waal energy in the above results. GLN(A)1010, GLN(A)1011, and GLN(A)762 interact with BMPTSC through strong hydrogen bonds. The

Table 3 MM-PBSA binding energy values of BMPTSC with the protein targets spike glycoprotein, ACE-2, endoribonuclease, and Mpro and its component energies. All reported energy values have a standard deviation within the range of 10 kJ/mol

Target	van der Waal energy (kJ/mol)	Electrostatic energy (kJ/mol)	Polar solvation energy (kJ/mol)	SASA energy (nonpolar solvation) (kJ/mol)	Binding energy (kJ/mol)
Spike Glycoprotein	−237.723	−81.839	161.180	−21.492	−179.874 +/− 9.1
ACE-2	−145.433	−22.454	39.542	−17.267	−145.611 +/− 9.6
Endoribonuclease	−155.075	−28.557	107.708	−18.004	−93.928 +/− 8.4
Mpro	−88.505	−17.028	60.860	−10.950	−55.623 +/− 8.3

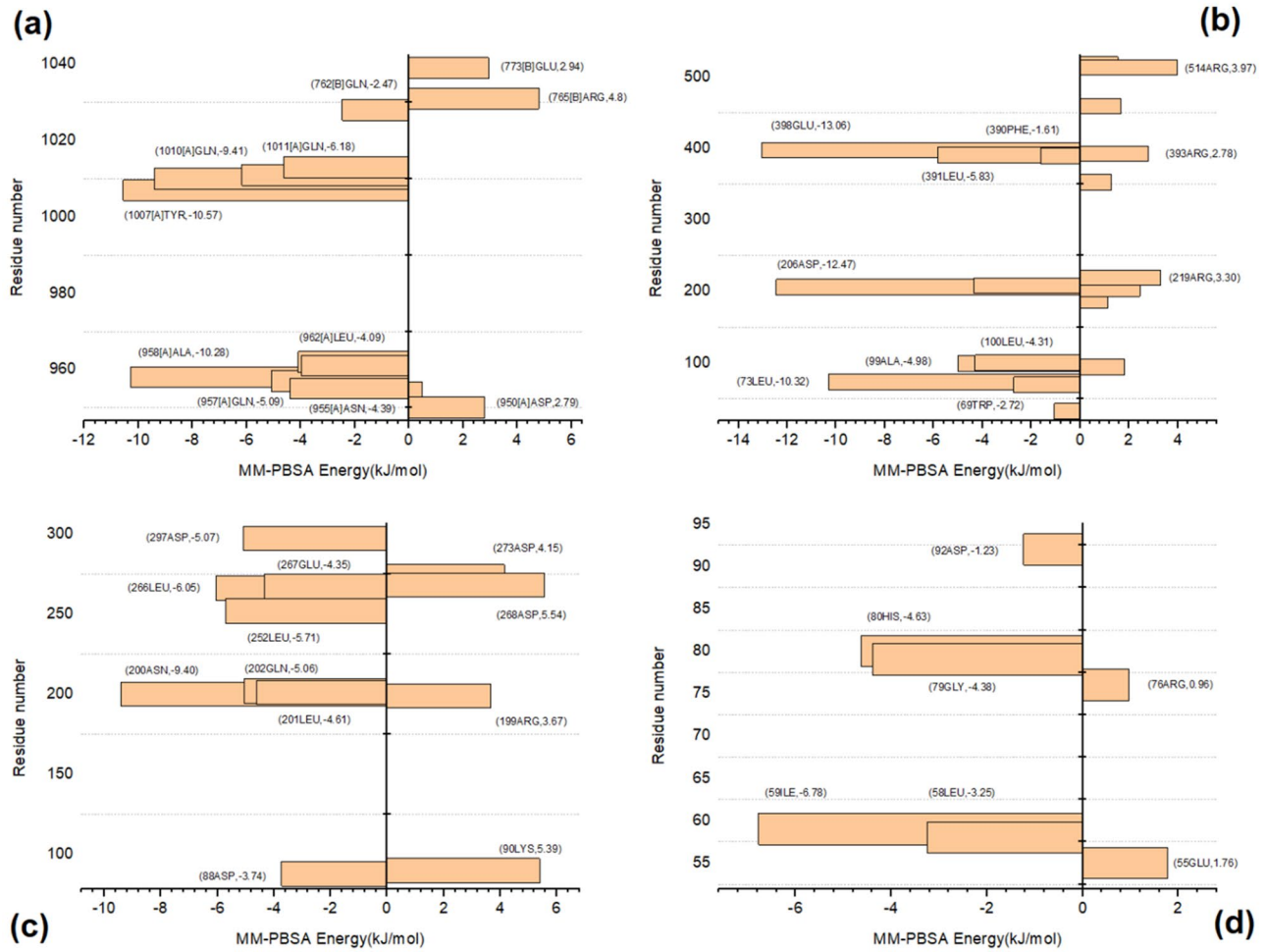

Fig. 8 MM-PBSA binding energy decomposition of residues of **a** spike glycoprotein in BMPTSC-spike glycoprotein complex, **b** ACE-2 in BMPTSC-ACE2 complex, **c** Nsp 15 in BMPTSC-Nsp 15 complex, and **d** MPro in BMPTSC-Mpro complex

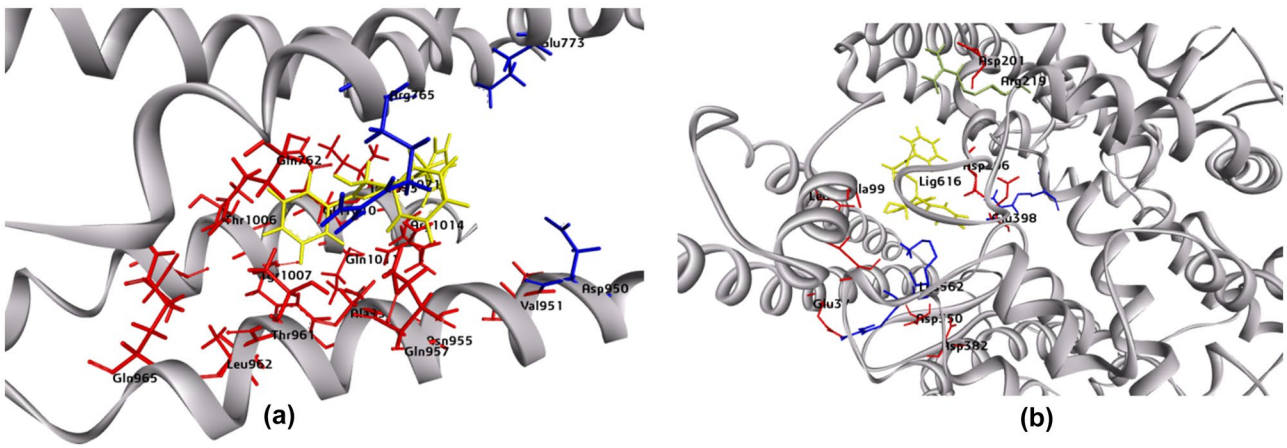

Fig. 9 Hot spot residues, bad contact residues, and ligand residue are indicated by red-, blue-, and yellow-colored stick representations respectively obtained from the MM-PBSA binding energy–residue decomposition analysis of **a** spike glycoprotein and (**b**) ACE-2 protein complex

negative energy values associated with the solvent accessible surface area also contribute to the total binding energy. However, the effective protein–ligand binding is hindered by the unfavorable interactions of some amino acid residues in the target with the ligand. The unfavorable interactions of blue spot residues ARG(B)765 (4.8 kJ/mol), GLU(B)773 (2.9 kJ/mol), and ASP(A)950 (2.8 kJ/mol) with ligand contributed positive value to the MM-PBSA binding energy by increasing polar solvation energies and may act against the effective protein–ligand binding.

We performed MM-PBSA energy decomposition analysis for BMPTSC-ACE-2 complex also. The crucial hot spot residues that contributed significantly in the protein–ligand binding of the complex are GLU398 (−13.0 kJ/mol), ASP206 (−12.47 kJ/mol), LEU73 (−10.32 kJ/mol), LEU391 (−5.83 kJ/mol), ALA99 (−4.98 kJ/mol), and LEU100 (−4.30 kJ/mol) respectively. Among these residues, all LEU and ALA residues interact with the ligand through hydrophobic interactions. However, the highly contributing glutamic acid and aspartic acid residues can interact through hydrogen bonding and other nonbonding interactions.

It may be noted that though docking scores of four protein–ligand complexes are comparable, a marked difference occurred in the MM-PBSA binding energy calculations. This discrepancy is mainly due to the difference in the nature of protein–ligand binding in the conformations obtained from long equilibrated MD trajectories compared to the initially used docking poses in simulations. As per the MM-PBSA results, we can finalize the inhibitory activity of BMPTSC against the four target proteins in the order: spike glycoprotein > ACE-2 Protein > Nsp 15 > Mpro.

In silico prediction of some drug designing parameters of BMPTSC

In this section, we describe various virtual screening strategies such as oral bioavailability, bioactivity scores, ADME, druglikeness, and medicinal chemistry friendliness properties of BMPTSC to understand the compactibility of this molecule as a versatile drug.

Modeling of oral bioavailability

Drug oral bioavailability, an important pharmacokinetic property, describes the fraction of an oral dose of the drug that reaches the systemic circulation and its site of action to provide its pharmacological and therapeutic effects. The computed physicochemical properties of BMPTSC leading to its oral bioavailability are given in Table 4.

As per Lipinski's rule of five, BMPTSC is found to be an orally bioavailable molecule as its logP value is 4.55 (less than 5), Molecular weight is 375.50 g/mol (less than 500), the number of hydrogen bond donor is 2 (less than 5), and the number of hydrogen bond acceptor is 4 (less than 10). It also satisfies extensions to Lipinski's rule of five, with the polar surface area given by 47.86 $Å^2$ (less than or equal to 140 $Å^2$) and the number of rotatable bonds equal to 7 (less than or equal to 10). This shows that BMPTSC obeyed Lipinski's rule of five, thereby ensuring good oral bioavailability.

Table 4 Physiochemical properties of BMPTSC

Properties	Values
miLogP	4.55
TPSA	47.86 $Å^2$
nAtoms	27
MW	375.50 g/mol
n ON	4
nOHNH	2
nViolations	0
nROTB	7
Volume	344.57 $Å^3$

Bioactivity score analysis

Table 5 displays the bioactivity scores of BMPTSC against different drug targets. The computed bioactivity scores of the studied molecule investigated for some important drug classes such as GPCR ligand, ion channel modulator, a kinase inhibitor, nuclear receptor ligand, protease inhibitor, and enzyme inhibitor show that BMPTSC exhibits moderate biological activity against all these targets, as revealed by the respective score which lies between −0.5 and 0.0.

ADME, medicinal chemistry friendliness, and druglikeness properties

ADME (absorption, distribution, metabolism, elimination) properties, druglikeness, and medicinal chemistry friendliness of BMPTSC calculated with SwissADME are summarized in Table 6.

Table 5 Bioactivity scores of BMPTSC against different drug targets

Targets	Bioactivity score
GPCR ligand	−0.26
Ion channel modulator	−0.29
Kinase inhibitor	−0.44
Nuclear receptor ligand	−0.19
Protease inhibitor	−0.24
Enzyme inhibitor	−0.12

In terms of partition coefficient between n-octanol and water (logP), lipophilicity of BMPTSC has been calculated by five different predictive models, viz., iLOGP, XLOGP3, WLOGP, MLOGP, and SILICOS-IT, available with SwissADME web tool. All the values are less than 5, and giving consensus logP, the arithmetic means of the five predicted values are equal to 3.92, satisfying the lipohilic nature of the compound under study. The water solubility of the molecule evaluated by the three topological methods, namely, the Esol model, Ali model, and SILICOS-IT, is −5.10, −6.01, and −6.87, respectively. ESOL model predicts moderate solubility, as the reference range of logS for moderate solubility is −4 to −6.

Several pharmacokinetic parameters of BMPTSC have been predicted; out of which, the most attractive one is the high gastrointestinal absorption, permitting for oral administration. Notably, the molecule is not a permeability glycoprotein (Pgp) substrate, the active efflux transporter. It shows inhibition towards CYP2C19, CYP2C9, and CYP2D6 enzymes whereas acts as non-inhibitor for CYP1A2 and CYP3A4 enzymes. A high negative value of skin permeability assures less skin permeation of the studied molecule. Also, the molecule is not at all blood brain barrier (BBB) permeable.

Table 6 ADME properties, druglikeness, and medicinal chemistry friendliness of BMPTSC

Property	Value
Lipophilicity	
logP (iLOGP)	3.01
logP (XLOGP3)	4.61
logP (WLOGP)	3.81
logP (MLOGP)	3.68
logP (SILICOS-IT)	4.50
Consensus logP	3.92
Water solubility	
logS (ESOL)	−5.10
logS (Ali)	−6.01
logS (SILICOS-IT)	−6.87
Pharmaokinetics	
GI absorption	High
BBB permeant	No
Pgp substrate	No
CYP1A2 inhibitor	No
CYP3A4 inhibitor	No
CYP2C19 inhibitor	Yes
CYP2C9 inhibitor	Yes
CYP2D6 inhibitor	Yes
$\log K_p$	−5.32 cm/s
Druglikeness	
Lipinski	Yes, 0 violation
Ghose	Yes
Veber	Yes
Egan	Yes
Muegge	Yes
Bioavailability score	0.55
Medicinal chemistry	
Leadlikeness	No, 2 violations: MW > 350,XLOGP > 3.5
Synthetic accessibility	3.80

The druglikeness indicating qualitative assessment of the molecule to be an oral drug with respect to bioavailability has been analyzed by five different rule-based filters such as Lipinski, Ghose, Veber, Egan, and Muegge, available in SwissADME tool. Bioavailability score of 0.55 further confirms the high potential of BMPTSC as a druglike molecule.

Medicinal chemistry friendliness parameter indicates moderately easy accessibility to synthesis this molecule of interest. However, it does not predict the molecule's leadlikeness as there are two violations given by MW > 350 and XLOGP > 3.5.

All the screening strategies adopted in this study highlights BMPTSC as a versatile drug candidate to combat the coronavirus threat. It should be further validated by in vitro and in vivo studies, leading to the design of this novel thiosemocarbazone as an effective drug for COVID-19 treatment.

Conclusions

This article presents the synthesis, structural characterization, and computational studies towards exploring 2-hydroxy-1,2-diphenylethanone N(4)-methyl-N(4) phenylthiosemicarbazone (BMPTSC) as a potential therapeutic against SARS-CoV-2, the causative organism for COVID-19. BMPTSC is a novel thiosemicarbazone that inhibits SARS-CoV-2 primarily via ACE-2 and spike glycoprotein inhibition. We identified the potential inhibitory activity of BMPTSC ligand against the spike glycoprotein and ACE-2 protein on account of the results obtained from molecular docking, MD trajectory analysis based on protein–ligand interactions and MM-PBSA binding energies. The MM-PBSA study also recognizes some of the key amino acid residues TYR(A)1007, ALA(A)958, GLN(A)1010, GLN(A)1011, GLN(A)957, ASN(A)955, LEU(A) 962, and GLN(A)762 of spike glycoprotein(6VXX) and GLU398, ASP206, LEU73, LEU391, ALA99, and LEU100 of ACE-2 protein (1R42) that may act as binding site residues for potential inhibitors. Virtual screening for oral bioavailability, bioactivity, ADME, druglikeness, pharmacokinetic properties, etc. provides supporting information regarding the pharmaceutical perspective of BMPTSC, which in turn facilitates the rational designing of a novel inhibitor targeting

COVID-19. In vitro and in vivo analyses are needed to validate the computational insights further and improve pharmacokinetics to fine-tune BMPTSC as a promising lead for COVID-19 drug discovery.

Supplementary Information The online version contains supplementary material available at https://doi.org/10.1007/s11224-022-02033-8.

Author contribution RJ and KKA designed the experimental part, performed the synthesis, analyzed, and interpreted the characterization data. APK performed the molecular docking studies, analyzed, and interpreted the data. TGA and JKV performed the molecular dynamics studies and interpreted the results. PKS provided the computational facilities for the MD studies. APK, RJ, and TGA prepared the manuscript and edited it by PKS.

Funding R. Jeevana is grateful to Council of Scientific and Industrial Research (CSIR), Govt. of India, for the research fellowship during the experimental part of this work. A. P. Kavitha and P. K. Sajith acknowledge DST-FIST and DST-SERB, Govt. of India, for providing financial assistance to Farook College and support through the grant ECR/2017/000524.

Availability of data and material All data analyzed during this work are included in this article/supporting information.

Code availability Not applicable.

Declarations

Conflict of interest The authors declare no competing interests.

References

1. Tong TR (2009) Drug targets in severe acute respiratory syndrome (SARS) virus and othercoronavirus infections. Infect Disord 9:223–245
2. Dayer MR (2017) Lopinavir; a potent drug against coronavirus infection: Insight from molecular docking study. Arch Clin Infect Dis 12:1–7
3. Adeyemi SGS, Adedeji O (2014) Antiviral drugs specific for coronaviruses in preclinical development. Curr Opin Virol 45–53
4. Fischer A, Sellner M, Neranjan S, Lill MA, Smieško M (2020) Inhibitors for novel coronavirus protease identified by virtual screening of 687 million compounds. Chem Rxiv Prepr 1–21
5. Zhang L, Lin D, Sun X, Curth U, Drosten C, Sauerhering L, Becker S, Rox K, Hilgenfeld R (2020) Crystal structure of SARS-CoV-2 main protease provides a basis for design of improved α-ketoamide inhibitors. Science 368:1–9
6. Zhang L, Lin D, Sun X, Rox K, Hilgenfeld R (2020) X-ray structure of main protease of the novel coronavirus SARS-CoV-2 enables design of α-Ketoamide inhibitors. BioRxiv. 1–14
7. Jin Z, Du X, Xu Y, Deng Y, Liu M, Zhang B, Li X, Zhang L, Peng C, Duan Y, Yu J, Yang K, Liu F, Jiang R, Yang X, You T, Liu X, Yang X, Bai F, Liu H, Liu X, Guddat LW, Xu W, Qin C, Shi Z, Jiang H, Rao Z, Yang H (2020) Structure of Mpro from COVID-19 virus and discovery of its inhibitors. BioRxiv 1–34
8. Liu X, Wang X (2020) Potential inhibitors for 2019-nCoV coronavirus M protease from clinically approved medicines. BioRxiv 1–12
9. ul Qamar MT, Alqahtani SM, Alamri MA, Chen LL (2020) Structural basis of SARS-CoV-2 3CLpro and anti-COVID-19 drug discovery from medicinal plants. J Pharm Anal 10:313–319
10. Martinez CM, Lezama AR (2020) Identification of potential inhibitors of SARS-CoV-2 main protease via a rapid in-silico drug repurposing approach. ChemRxiv 1–13
11. Khaerunnisa S, Kurniawan H, Awaluddin R, Suhartati S, Soetjipto S (2020) Potential inhibitor of COVID-19 main protease (M pro) from several medicinal plant compounds by molecular docking study. Preprints 1–14
12. Sekhar T (2020) Virtual Screening based prediction of potential drugs for COVID-19. Comb Chem High Throughput Screen 24:716–728
13. Sepay N, Al Hoque A, Mondal R, Halder UC, Muddassir M (2020) In Silico fight against novel coronavirus by finding chromone derivatives as inhibitor of coronavirus main proteases enzyme. Struct Biol Bioinforma 1–24
14. Arya R, Das A, Prashar V, Kumar M (2020) Potential inhibitors against papain-like protease of novel coronavirus (SARS-CoV-2) from FDA approved drugs. Chemrxiv Org 1–8
15. Deng X, Baker SC (2018) An "Old" protein with a new story: coronavirus endoribonuclease is important for evading host antiviral defenses. Virology 517:157–163
16. Ou X, Liu Y, Lei X, Li P, Mi D, Ren L, Guo L, Guo R, Chen T, Hu J, Xiang Z, Mu Z, Chen X, Chen J, Hu K, Jin Q, Wang J, Qian Z (2020) Characterization of spike glycoprotein of SARS-CoV-2 on virus entry and its immune cross-reactivity with SARS-CoV. Nat Commun 11:1–12
17. Wang M, Cao R, Zhang L, Yang X, Liu J, Xu M, Shi Z, Hu Z, Zhong W, Xiao G (2020) Remdesivir and chloroquine effectively inhibit the recently emerged novel coronavirus (2019-nCoV) in vitro. Cell Res 30:269–271
18. Tan ELC, Ooi EE, Lin CY, Tan HC, Ling AE, Lim B, Stanton LW (2004) Inhibition of SARS coronavirus infection in vitro with clinically approved antiviral drugs. Emerg Infect Dis 10:581–586
19. Junmei WJ (2020) Fast identification of possible drug treatment of coronavirus disease -19 (COVID-19) through computational drug repurposing study. Chem Inf Model 53:1689–1699
20. Contini A (2020) Virtual screening of an FDA approved drugs database on two COVID-19 coronavirus proteins. Preprint 1–7
21. Zhu Z, Wang X, Yang Y, Zhang X, Mu K, Shi Y, Peng C, Xu Z, Zhu W (2020) D3 Similarity : A ligand-based approach for predicting drug targets and for virtual screening of active compounds against COVID-19. Chemrxiv 1–15. https://doi.org/10.26434/chemrxiv.11959323.v1
22. Varughese JK, Libin KLJ, Sindhu KS, Rosily AV, Abi TG (2021) Investigation of the inhibitory activity of some dietary bioactive flavonoids against SARS-CoV-2 using molecular dynamics simulations and MM-PBSA calculations. J Biomol Struct Dyn 1–16
23. Beck BR, Shin B, Choi Y, Park S, Kang K (2020) Predicting commercially available antiviral drugs that may act on the novel coronavirus (SARS-CoV-2) through a drug-target interaction deep learning model. Comput Struct Biotechnol J 18:784–790
24. Zhavoronkov A, Zhebrak A, Zagribelnyy BA, Bezrukov D (2020) Potential 2019-nCoV 3C-like protease inhibitors designed using generative deep learning approaches. ChemRxiv Preprint. 1–19
25. Bauer DJ (1973) Antiviral Chemotherapy: The first decade. Br Med J 3:275–279
26. Bauer DJ (1955) The antiviral and synergic actions of isatin thiosemicarbazone and certain phenoxypyrimidines in vaccinia infection in mice. Br J Ex Pathol 36:105–114
27. Bauer DJ (1965) Clinical experience with the antiviral drug marboran (1-methylisatin 3-thiosemicarbazone). Ann N Y Acad Sci. https://doi.org/10.1111/j.1749-6632.1965.tb12545.x
28. Heffeter P, Pape VFS, Enyedy ÉA, Keppler BK, Szakacs G, Kowol CR (2019) Anticancer thiosemicarbazones: chemical properties,

interaction with iron metabolism, and resistance development. Antioxid Redox Signal 30:1062–1082
29. Haribabu J, Subhashree GR, Saranya S, Gomathi K, Karvembu R, Gayathri D (2016) Isatin based thiosemicarbazone derivatives as potential bioactive agents: antioxidant and molecular docking studies. J Mol Struct 1110:185–195
30. Ghosh S, Misra AK, Bhatia G, Khan MM, Khanna AK (2009) Syntheses and evaluation of glucosyl aryl thiosemicarbazide and glucosyl thiosemicarbazone derivatives as antioxidant and antidyslipidemic agents. Bioorganic Med Chem Lett 19:386–389
31. Tenório RP, Carvalho CS, Pessanha CS, De Lima JG, De Faria AR, Alves AJ, De Melo EJT, Góes AJS (2005) Synthesis of thiosemicarbazone and 4-thiazolidinone derivatives and their in vitro anti-Toxoplasma gondii activity. Bioorganic Med Chem Lett 15:2575–2578. https://doi.org/10.1016/j.bmcl.2005.03.048
32. Bharti N, Husain K, Garza MTG, Cruz-vega DE, Mata-cardenas BD, Azam A (2002) Synthesis and in vitro antiprotozoal activity of thiosemicarbazone derivatives. Bioorg Med Chem Lett 12:3475–3478
33. de Oliveira RB, de Souza-Fagundes EM, Soares RPP, Andrade AA, Krettli AU, Zani CL (2008) Synthesis and antimalarial activity of semicarbazone and thiosemicarbazone derivatives. Eur J Med Chem 43:1983–1988
34. Shailendra NS, Bharti N, Garza MTG, Cruz-Vega DE, Garza JC, Saleem K, Naqvi F, Azam A (2001) Synthesis, characterisation and antiamoebic activity of new thiophene-2-carboxaldehyde thiosemicarbazone derivatives and their cyclooctadiene Ru(II) complexes. Bioorganic Med Chem Lett 11:2675–2678
35. Dimmock J, McColl J, Wonko S, Thayer R, Hancock D (1991)). Evaluation of the thiosemicarbazones of some aryl alkyl ketones and related compounds for anticonvulsant activities. Eur J Med Chem 26:529–534
36. Priya NP, Firdous AP, JeevanaR AKK (2015) Cytotoxic and antitumour studies of acetoacetanilide N(4)-methyl(phenyl)thiosemicarbazone and its transition metal complexes. Indian J Pharm Sci 77:655–660
37. He Z, Qiao H, Yang F, Zhou W, Gong Y, Zhang X, Wang H, Zhao B, Ma L, min Liu H, Zhao W (2019) Novel thiosemicarbazone derivatives containing indole fragment as potent and selective anticancer agent. Eur J Med Chem 184:111764
38. Sardroud SJ, Hosseini-Yazdi SA, Mahdavi M, Poupon M, Skorepova E (2020) Synthesis, characterization and in vitro evaluation of anticancer activity of a new water-soluble thiosemicarbazone ligand and its complexes. Polyhedron 175:114218
39. de Clercq E (2010) Historical perspectives in the development of antiviral agents against poxviruses. Viruses 2:1322–1339
40. Shipman C, Smith SH, Drach JC, Klayman DL (1981) Antiviral thiosemicarbazones. Antimicrob Agents Chemother 19:682–685
41. Kesel AJ (2011) Broad-spectrum antiviral activity including human immunodeficiency and hepatitis C viruses mediated by a novel retinoid thiosemicarbazone derivative. Eur J Med Chem 46:1656–1664
42. Padmanabhan P, Khaleefathullah S, Kaveri K, Palani G, Ramanathan G, Thennarasu S, Sivagnanam UT (2017) Antiviral activity of thiosemicarbazones derived from α-amino acids against Dengue virus. J Med Virol 89:546–552
43. Kang IJ, Wang LW, Hsu TA, Yueh A, Lee CC, Lee YC, Chao YS, Shih SR, Chern JH (2011) Isatin-β-thiosemicarbazones as potent herpes simplex virus inhibitors. Bioorganic Med Chem Lett 21:1948–1952
44. Afrasiabi Z, Sinn E, Chen J, Ma Y, Rheingold AL, Zakharov LN, Rath N, Padhye S (2004) Appended 1,2-naphthoquinones as anticancer agents 1: Synthesis, structural, spectral and antitumor activities of ortho-naphthaquinone thiosemicarbazone and its transition metal complexes. Inorganica Chim Acta 357:271–278
45. Kovala-Demertzi D, Miller JR, Kourkoumelis N, Hadjikakou SK, Demertzis MA (1999) Palladium(II) and platinum(II) complexes of pyridine-2-carbaldehyde thiosemicarbazone with potential biological activity. Synthesis, structure and spectral properties. Extended network via hydrogen bond linkages of [Pd(PyTsc)Cl]. Polyhedron 18:1005–1013
46. Soares MA, Lessa JA, Mendes IC, Da Silva JG, Dos Santos RG, Salum LB, Daghestani H, Andricopulo AD, Day BW, Vogt A, Pesquero JL, Rocha WR, Beraldo H (2012) N 4-Phenyl-substituted 2-acetylpyridine thiosemicarbazones: cytotoxicity against human tumor cells, structure-activity relationship studies and investigation on the mechanism of action. Bioorganic Med Chem 20:3396–3409
47. West DX, Ives JS, Krejci J, Salberg MM, Zumbahlen TL, Bain GA, Liberta AE, Valdes-Martinez J, Hernandez-Ortiz S, Toscano RA (1995) Copper(II) complexes of 2-benzoylpyridine 4N-substituted thiosemicarbazones. Polyhedron 14:2189–2200
48. West DX, Ooms CE, Saleda JS, Gebremedhin H, Liberta AE (1994) Copper(II) and nickel(II) complexes of 2-formylpyridine 3-piperidinyl-, 3-hexamethyleneiminyl- and 3-azabicyclo[3.2.2] nonylthiosemicarbazones. Transition Met Chem 19:553–558
49. Scovill JP, Klayman DL, Franchino CF (1982) 2-Acetylpyridine thiosemicarbazones. 4. Complexes with transition metals as antimalarial and antileukemic agents. J Med Chem 25:1261–1264
50. Vosko SH, Wilk L, Nusair M (1980) Accurate spin-dependent electron liquid correlation energies for local spin density calculations: a critical analysis. Can J Phys 58:1200–1211
51. Lee C, Yang W, Parr RG (1998) Development of the Colle-Salvetti correlation-energy formula into a functional of the electron density. Phys Rev B 37:785–789
52. Frisch MJ, Trucks GW, Schlegel HB, Scuseria GE, Robb MA, Cheeseman JR, Scalmani G, Barone V, Mennucci B, Petersson GA, Nakatsuji H, Caricato M, Li X, Hratchian HP, Izmaylov AF, Bloino J, Zheng G, Sonnenberg JL, Hada M, Ehara M, Toyota K, Fukuda R, Hasegawa J, Ishida M, Nakajima T, Honda Y, Kitao O, Nakai H, Vreven T, Montgomery JA, Peralta JE, Ogliaro F, Bearpark M, Heyd JJ, Brothers E, Kudin KN, Staroverov VN, Kobayashi R, Normand J, Raghavachari K, Rendell A, Burant JC, Iyengar SS, Tomasi J, Cossi M, Rega N, Millam JM, Klene M, Knox JE, Cross JB, Bakken V, Adamo C, Jaramillo J, Gomperts R, Stratmann RE, Yazyev O, Austin AJ, Cammi R, Pomelli C, Ochterski JW, Martin RL, Morokuma K, Zakrzewski VG, Voth GA, Salvador P, Dannenberg JJ, Dapprich S, Daniels AD, Farkas O, Foresman JB, Ortiz JV, Cioslowski J, Fox DJ (2009) Gaussian 09, Revision B01. Guassian Inc, Wallingford
53. Molinspiration Cheminformatics free web services, https://www.molinspiration.com, Slovensky Grob, Slovakia
54. Daina A, Michielin O, Zoete V (2017) SwissADME: a free web tool to evaluate pharmacokinetics, drug-likeness and medicinal chemistry friendliness of small molecules. Sci Rep 7:1–13
55. Trott O, Olson AJ (2010) AutoDock Vina: Improving the speed and accuracy of docking with a new scoring function, efficient optimization, and multithreading. J Comput Chem 31:455–461
56. Wang Y, Xiao J, Suzek TO, Zhang J, Wang J, Bryant SH (2009) A public information system for analyzing bioactivities of small molecules. Nucleic Acids Res 37:623–633
57. Morris GM, Huey R, Lindstrom W, Sanner MF, Belew RK, Goodsell DS, Olson AJ (2009) Autodock4 and AutoDock Tools4: automated docking with selective receptor flexibility. J Comput Chem 16:2785–2791
58. BIOVIA (2016) Dassault Systemes, Discovery Studio visualizer v16.1.0.15350, San Diego: Dassault Systemes. Accessed 10 Jan 2021
59. Berendsen HJC, van der Spoel D, van Drunen R (1995) GROMACS: A message-passing parallel molecular dynamics implementation. Comput Phys Commun 43–56

60. Jorgensen WL, Maxwell DS, Tirado-Rives J (1996) Development and testing of the OPLS all-atom force field on conformational energetics and properties of organic liquids. J Am Chem Soc 118:11225–11236
61. Dodda LS, Cabeza de Vaca I, Tirado-Rives J, Jorgensen WL (2017) LigParGen web server: an automatic OPLS-AA parameter generator for organic ligands. Nucleic Acids Res 45(W1):W331–W336
62. Toukan K, Rahman A (1985) Molecular-dynamics study of atomic motions in water. Phys Rev B 31:2643–2648
63. Loup V (1967) Computer "experiments" on classical fluids. I. Thermodynamical properties of Lennard–Jones molecules. Phys Rev 159:98
64. Di Pierro M, Elber R, Leimkuhler B (2015) A stochastic algorithm for the isobaric–isothermal ensemble with ewald summations for all long range forces. J Chem Theory Comput 11:5624–5637
65. Hess B (2008) A parallel linear constraint solver for molecular simulation. J Chem Theory Comput 4:116–122
66. Kollman PA, Massova I, Reyes C, Kuhn B, Huo S, Chong L, Lee M, Lee T, Duan Y, Wang W, Donini O, Cieplak P, Srinivasan J, Case DA, Cheatham TE (2000) Calculating structures and free energies of complex molecules: combining molecular mechanics and continuum models. Acc Chem Res 33:889–897
67. Wang E, Sun H, Wang J, Wang Z, Liu H, Zhang JZH, Hou T (2019) End-point binding free energy calculation with MM/PBSA and MM/GBSA: strategies and applications in drug design. Chem Rev 119:9478–9508
68. Kumari R, Kumar R, Lynn A (2014) g_mmpbsa—a GROMACS tool for high-throughput MM-PBSA calculations. J Chem Inf Model 54:1951–1962
69. Marimuthu P, Singaravelu K (2018) Prediction of hot spots at myeloid cell leukemia-1–inhibitor interface using energy estimation and alanine scanning mutagenesis. Biochemistry 57:1249–1261
70. Zoete V, Irving MB, Michielin O (2010) MM–GBSA binding free energy decomposition and T cell receptor engineering. J Mol Recognit 23:142–152
71. Lipinski CA, Lombardo F, Dominy BW, Feeney PJ (2001) Experimental and computational approaches to estimate solubility and permeability in drug discovery and development settings. Adv Drug Deliv Rev 46:3–26
72. Veber DF, Johnson SR, Cheng HY, Smith BR, Ward KW, Kopple KD (2002) Molecular properties that influence the oral bioavailability of drug candidates. J Med Chem 45:2615–2623
73. Lu JJ, Crimin K, Goodwin JT, Crivori P, Orrenius C, Xing L, Tandler TJ, Vidmar PJ, Amore BM, Wilson AGE, Stouten PFW, Burton PS (2004) Influence of molecular flexibility and polar surface area metrics on oral bioavailability in the rat. J Med Chem 47:6104–6107
74. Ertl P, Rohde B, Selzer P (2000) Fast calculation of molecular polar surface area as a sum of fragment based contributions and its application to the prediction of drug transport properties. J Med Chem 43:3714–3717
75. Hassan B, Shireen A, Muraleedharan K, Mujeeb VMA (2015) Virtual screening of molecular properties of chitosan and derivatives in search for druggable molecules. J Biol Macromol 74:392–396
76. Patil R, Das S, Stanley A, Yadav L, Sudhakar A, Varma AK (2010) Optimized hydrophobic interactions and hydrogen bonding at the target-ligand interface leads the pathways of drug-designing. PLoS ONE 5:1–10
77. De Freitas RF, Schapira M (2017) A systematic analysis of atomic protein-ligand interactions in the PDB. Medchemcomm 8:1970–1981
78. Raschka S, Wolf AJ, Bemister-Buffington J, Kuhn LA (2018) Protein–ligand interfaces are polarized: discovery of a strong trend for intermolecular hydrogen bonds to favor donors on the protein side with implications for predicting and designing ligand complexes. J Comput Aided Mol Des 32:511–528
79. Maximilian S, Peter R, Marc S, Rafael CB, Klaus S, Emad T, Till R (2018)). PyContact: rapid, customizable, and visual analysis of noncovalent interactions in MD simulations. Biophys J 114:577–583
80. Ismail TM, Mohan N, Sajith PK (2021) Theoretical study of hydrogen bonding interactions in substituted nitroxide radicals. New J Chem 45:3866–3875